






Article

Experimental Assessment of the Efficiency of Two-Phase Ejector Components for Isobutane

Kamil Śmierciew ¹, Adam Dudar ¹, Dariusz Butrymowicz ^{1,*}, Jerzy Gagan ¹, Paweł Jakończuk ¹
and Huiming Zou ²

¹ Faculty of Mechanical Engineering, Białystok University of Technology, 15-351 Białystok, Poland

² Technical Institute of Physics and Chemistry, Chinese Academy of Sciences, Beijing 100045, China

* Correspondence: d.butrymowicz@pb.edu.pl

Abstract: Two-phase ejectors as well as single phase ejectors can be applied in many branches of industry: refrigeration and heat pump systems, chemical engineering, food processing, and others. Due to the complicated nature of the process of momentum transfer in two-phase ejectors, their design procedure based on the accurate theoretical prediction of the ejector performance is still an open issue. The paper provides its own experimental results of the velocity coefficients of the components of the two-phase ejector, i.e., the motive nozzle, suction chamber, mixing chamber, and diffuser. The results were obtained in the case of isobutane as the working fluid. It was demonstrated that the velocity coefficients may not be treated as constant quantities. Therefore, our own proposed dimensionless relationships describe the velocity coefficients of the components of the ejector that may be applied in the design procedure of the ejector. The two physical parameters, the wet vapour quality and the volumetric entrainment ratio, were selected as the key parameters. In addition, the aspects of the prediction of the critical mass flow rate of the motive nozzles was considered on the basis of the Henry–Fauske model. It was demonstrated that the model accurately predicts the two-phase critical flow under the conditions of a higher range of wet vapour quality.

Keywords: two-phase ejector; refrigeration; isobutane; velocity coefficient; critical flow; natural working fluids



check for updates

Citation: Śmierciew, K.; Dudar, A.; Butrymowicz, D.; Gagan, J.; Jakończuk, P.; Zou, H. Experimental Assessment of the Efficiency of Two-Phase Ejector Components for Isobutane. *Sustainability* **2022**, *14*, 13356. <https://doi.org/10.3390/su142013356>

Academic Editor: Adrián Mota Babiloni

Received: 10 September 2022

Accepted: 11 October 2022

Published: 17 October 2022

Publisher's Note: MDPI stays neutral with regard to jurisdictional claims in published maps and institutional affiliations.



Copyright: © 2022 by the authors. Licensee MDPI, Basel, Switzerland. This article is an open access article distributed under the terms and conditions of the Creative Commons Attribution (CC BY) license (<https://creativecommons.org/licenses/by/4.0/>).

1. Introduction

The application of two-phase ejectors is a promising way to increase thermal system efficiency and utilise low-grade heat as a tool for the development of a sustainable energy conversion approach. Depending on the type, the ejectors can be used in many branches of industry, e.g., the separation of substances at the vapour phase and the production of solvents, chemical products, and fumes. The most popular applications are air-conditioning, refrigeration, and chemical engineering [1]. Depending on the configuration of the refrigeration systems, the ejector can be applied in absorption systems or compression systems and can operate as a first- or second-step compression device [2]. In the first discussed case, the ejector operates at relatively low temperatures in a suction chamber inlet as the ejector entrains vapour from the evaporator. In the second case, the ejector operates at high temperatures, especially in the suction chamber, as the ejector entrains vapour discharged from a compressor. It is expected that numerous applications of the two-phase ejectors need performance improvement. Recently, the application of the two-phase ejector in the liquid line in refrigeration and heat pump systems has been considered as one of the most efficient approaches [2,3]. However, due to the different thermodynamic properties of perspective and environmentally friendly natural fluids in comparison with numerous synthetic substances, the possibilities of the application of natural working fluids need many potential problems to be solved, e.g., the design of the ejector geometry and the prediction of its performance [4–6]. To date, there is still a lack of sufficient knowledge

regarding the operation of compression–ejector refrigeration systems as well as the physical phenomena occurring in the two-phase ejectors, especially for natural fluids other than carbon dioxide.

Much of the recent work on two-phase ejectors has been focused on the transcritical CO₂ cycles as this substance has a larger throttling loss than most other refrigerants [7–12]. In addition, recently, the refrigerants R134a and R1234yf in refrigeration applications with ejectors have been investigated more [13–16]. The analytical model of the operation of the two-phase ejector in the system requires the efficiencies of the main parts of the ejector to be known [17]. In general, the efficiencies of the main parts of the ejector are treated as constant quantities that do not depend on geometry or operation parameters. However, the applied geometry of the ejector components may be thought of as crucial for the performance of the ejector. The effects of the ejector geometry on its performance in the case of the ejector–expansion air conditioner with refrigerant R410A was demonstrated by Jeon et al. [18]. The effect of the motive nozzle diameter on the performance of the two-phase ejector for the refrigerant R-123 was presented by Butrymowicz et al. [19]. The most advanced theoretical model for the two-phase ejector as an expansion device has been performed by Ringstad et al. [20] and Wilhelmsen et al. [21]. The positive assessment of the applicability of the homogeneous equilibrium model (HEM) to predict the operation of the motive nozzle of the ejector was presented by Ameer et al. [22]. Palacz et al. [12] showed a comparison of the accuracy of the HEM and HRM models for a CO₂ expansion ejector cycle simulation. The results of the numerical modelling of the two-phase ejector using CFD techniques were presented by Banasiak et al. [23] and Yazdani et al. [24]. They compared the pressure profiles along the mixer and diffuser walls, and the entrainment ratios were compared with test data; the obtained deviation of the numerical and experimental results was approx. 10%. The CFD techniques can be thought of as a practical design tool; however, it requires the integration of separate submodels, e.g., a two-phase sonic velocity with a CFD code through user-defined functions. The experimental investigations of a transcritical CO₂ heat pump with ejector expansion was presented by Zhu et al. [25]. They demonstrated that the COP of the ejector–expansion system was 10.3% higher than for the corresponding basic cycle. In the papers [26–28], the experimental results of the application of the two-phase ejector as an expansion device for R-134a and R1234yf were presented. The results showed that ejectors designed for low-pressure fluids were able to achieve similar but lower work recovery efficiencies compared to the CO₂ ejectors. The experimental results of the improvement in the COP of the split air-conditioning system due to the application of a two-phase ejector as a throttling device instead of a capillary tube was presented by Sumeru et al. [29].

The investigations mentioned above, in most cases, dealt with the performance of the entire compression–refrigeration system or were dedicated to an individual part of the ejector, e.g., the motive nozzle. In spite of the intensive progress within the last twenty years, the accuracy of the theoretical prediction of two-phase ejector performance may be thought of as still insufficient compared with experimental results. There is a clear need for further investigation to better understand the physical phenomena and operation of the ejector. In addition, more experimental studies must be conducted, especially on a large scale, if good results in real applications are desired. The literature review showed that thermodynamic modelling methods are the most widespread for the two-phase ejector design. The majority of the models presented in the literature require assumptions of the efficiency of the ejector components, i.e., the motive nozzle, suction and mixing chambers, and diffuser.

In the literature, the velocity coefficients (corresponding to the efficiency) were assumed as constant quantities. Although such a simplified approach may be acceptable for a single phase ejector, it is not acceptable, as a general rule, in the case of two-phase ejectors. This is due to the very complex flow phenomena in two-phase ejectors as a result of the mixing process of the two phases, the formation of the mixing shock wave in the mixing chamber of the ejector as well as the significant changes of the two-phase flow pattern along

the flow path in the ejector. The motivation of the present research is the experimental assessment of the efficiencies of the ejector components in the case of isobutane as the working fluid.

Isobutane, as a natural substance that does not deplete the ozone layer and has a negligible warming impact ($GWP = 3.3$), is treated as a perspective refrigerant in numerous applications. Moreover, due to its advantageous thermodynamic and thermokinetic properties, it is already applied in numerous domestic refrigeration systems, air-conditioners, and others. The selection of the tested substance was based on legal and operational issues. Isobutane fulfils all of the restrictive requirements stated by the (EU) regulation no. 517/2014. It is also an environmentally friendly refrigerant.

As the velocity coefficients are not constant, the development of the dimensionless relationships were proposed on the basis of the experimental data. Therefore, the novelties proposed in this paper are our own developed correlations based on the experimental investigations of the two-phase ejector. The wide range of operating parameters make the obtained results versatile. The proposed correlations can be applied for the modelling of the general purpose two-phase ejectors. Another novelty is a new approach in terms of the estimation of the velocity coefficient of nozzles operating with wet vapour. To the knowledge of the authors, the general correlations developed for the two-phase liquid-vapour ejector operating with isobutane are not available in the professional literature. Another intriguing aspect of the application of the two-phase ejectors is the problem of the prediction of the critical mass flow rate. Although we can observe significant progress in the development of the CFD numerical approach based on thermodynamic nonequilibrium models, an engineering approach is still required for application in the design procedure of the two-phase ejector. The commonly applied semiempirical models developed for critical wet steam are lacking in the literature assessments of the applicability for refrigeration ejectors. One of commonly applied models of critical flow is the semiempirical model proposed by Henry and Fauske [30], e.g., for the design of safety valves in steam systems. Clearly, the applicability of such a model for the prediction of the critical flow in the motive nozzles of two-phase ejectors is one of the intriguing aspects that has not been considered in the literature to date. Therefore, the additional issue presented in this paper is the assessment of the prediction of the Henry–Fauske model [30] for the critical mass flow rate of the motive nozzles of the two-phase ejector operating with isobutane as the working fluid.

2. Experimental Apparatus and Procedure

The test facilities were designed and built for the investigations of ejector refrigeration system operating with natural working fluids; isobutane was used in this case. The schematic diagram of the experimental stand equipped with the ejector is shown in Figure 1, and schematic diagram of tested two-phase ejector is presented in Figure 2. Dimensions of the ejector are: D_{nt} —variable (see Table 1), $L_m = 40$ mm, $L_d = 68.5$ mm, $D_m = 6$ mm, L_{no} —variable, and $\varphi_d = 6^\circ$. The ejector shown in Figure 2 was equipped with several types of nozzle geometries during experiments. Detailed information about geometry of the tested nozzles is provided in Table 1 and Figure 3.

Table 1. Diameters of the tested nozzles in two-phase ejector.

Nozzle	Type	Throat Diameter D_{nt} [mm]	Outlet Diameter D_{no} [mm]
1	de Laval, Figure 3a, without orifice	1.0	2.4
2	de Laval, Figure 3a, with orifice	1.0	2.4
3	de Laval, Figure 3b	1.0	3.1
4	de Laval, geometry similar to Figure 3b	2.0	3.4
5	de Laval, Figure 3c	1.4	4.1
6	de Laval, Figure 3d	1.5	2.7
7	de Laval, Figure 3e	1.5	2.7
8	sharp edged, Figure 3f	1.0	1.0
9	sharp edged, Figure 3g	1.5	1.5

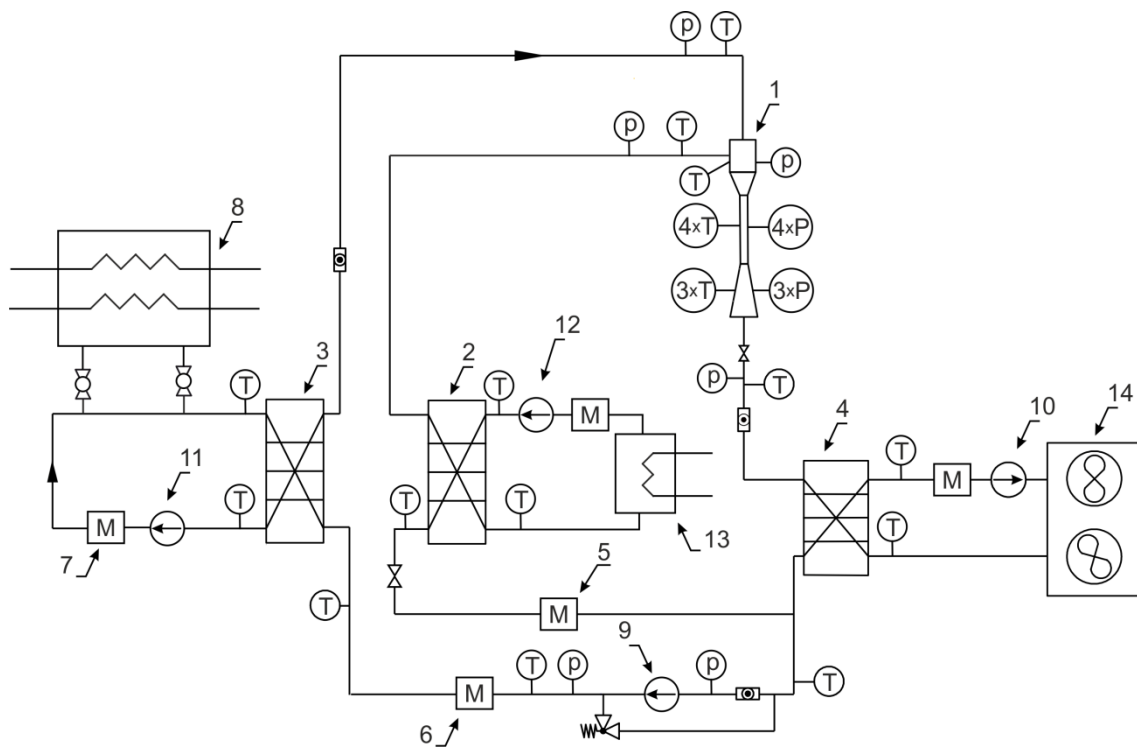


Figure 1. Schematic of the testing stand: 1—tested two-phase ejector; 2—evaporator; 3—preheater/vapour generator; 4—condenser; 5, 6, 7—mass flow meters; 8, 13—electric heaters; 9, 10, 11, 12—circulation pumps; and 14—dry cooler.

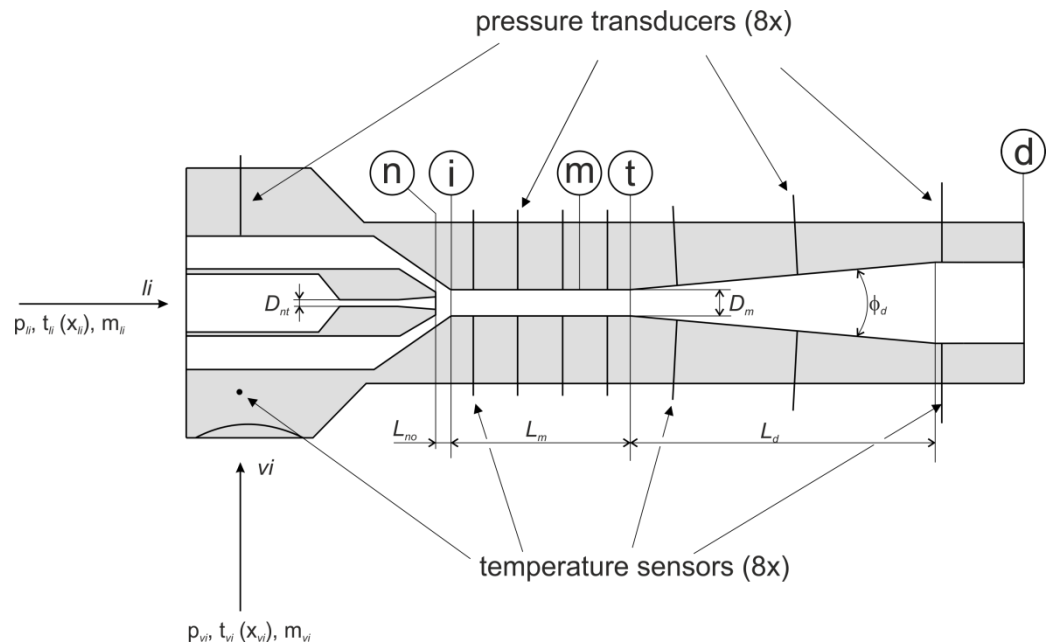


Figure 2. Schematic diagram of the tested two-phase ejector.

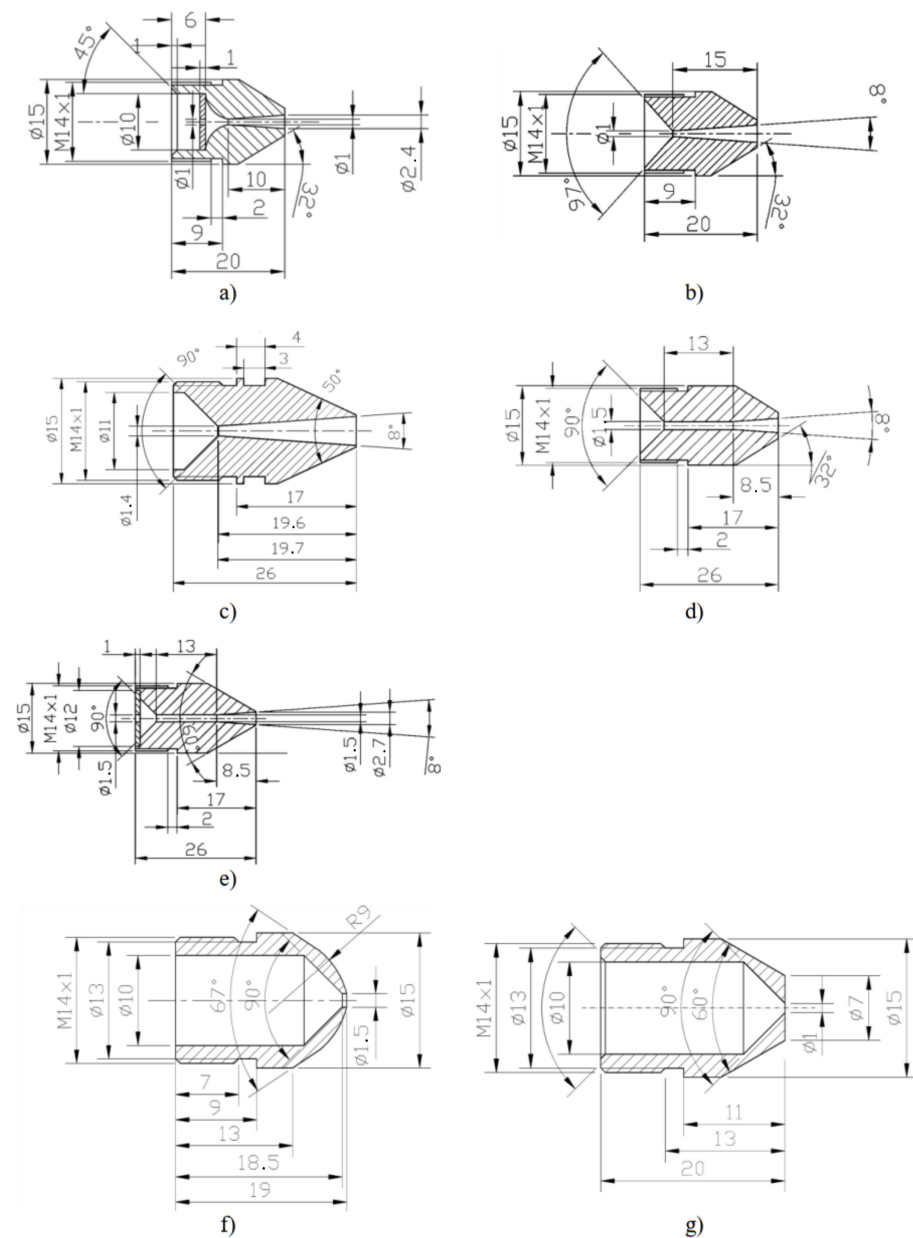


Figure 3. Geometries of the tested motive nozzles of the ejector; see Table 1.

During experiments, the motive nozzle was fed by saturated liquid. Pressure of motive liquid p_{li} was variable, and temperature of the motive liquid was in range between $t_{li} = 40 \div 80$ °C. During experiments, the mass flow rate of the motive liquid was in range $m_{li} = 50 \div 110$ kg/h. Pressure in suction chamber p_{vi} was equal to the evaporation saturation pressure. Temperature of evaporation varied up to 35 °C. Temperature of condensation was controlled by air-cooler during experiments, and it was fixed at constant level of 40 °C. This range of temperatures of the primary and secondary streams can be thought of as appropriate for investigation of operation of the all-purpose ejectors in many configurations of refrigeration systems.

Depending on the thermodynamic properties of the fluid, the pressure ratio p_{vi}/p_{li} in the experimental conditions was lower than gas-dynamic critical pressure ratio. Therefore, use of the supercritical de Laval nozzle was well-founded. It is worth noting that in two-phase ejector, the metastable flow with lack of equilibrium evaporation process during expansion in the nozzle can be observed. In this case, the flow disturb facilities such as orifices can help with initiation of the flashing vaporisation. Therefore, the special

orifice plate located at the nozzle inlet can be thought of as a good practice. In presented experimental investigations, the orifice plate with 1.0 mm and 1.5 mm opening diameters was used with the de Laval nozzle; see Table 1, nozzle no. 2 and no. 7.

The testing rig was equipped with temperature sensors and pressure transducers installed at the critical locations and other locations of interest. The pressure transducers with accuracy of 0.25% of the measurement range were used during the experiments. First-class K-type thermocouples were applied for the temperature measurement. The thermocouples were calibrated with total accuracy of ± 0.2 K. The Coriolis mass flow meters with an accuracy 0.15% of the measurement range were used. Sight-glasses were installed at various locations to observe the flow pattern at the inlets and outlet of tested ejector. The plate heat exchangers and the diaphragm pump for refrigerant circulation were used.

The testing rig was equipped with two additional loops: the first one for the thermal load of the evaporator and the second one for the condenser cooling. Centrifugal pumps were applied in the additional loops. These systems allow for the adjustment of the flow rates as well as for changing the operation parameters in a wide range. The condenser cooling system used the automatically controlled dry cooler. The thermal load system was equipped with the automatically controlled electric heater. The data acquisition system logged all main parameters and controlled valves, pumps, electric heaters, and safety system. For each of the experimental runs with all of the parameters fixed, 100 readings under steady-state conditions were taken and averaged to make one experimental point. Note that the presented part of the research did not cover analysis of the individual performance characteristics of the ejector but only the assessment of the efficiencies of the ejector components. Therefore, in the analysis, there were taken into account a total of 2830 experimental points which were covered and provided above range of the operation parameters.

3. Model of the Two-Phase Ejector

3.1. Prediction of the Critical Flow in the Two-Phase Motive Nozzle

One of the most important features of the operation of a two-phase ejector is the mass flow rate of the motive nozzle. This issue is related to the partial evaporation that occurs in the nozzle. For the estimation of the critical parameters in the two-phase flow, the Henry–Fauske model [30] is the most popular approach. However, this model was originally developed for wet steam, and it is commonly applied, e.g., for the design of wet steam safety valves. The present research is the first investigation of the applicability of this model to predict the critical mass flow rate of isobutane wet vapour. Therefore, in our research calculation procedure, the isentropic exponent of the saturated vapour was used instead of the Poisson constant as it is in the original Henry–Fauske model formulation [30]. The NIST database of the fluid thermodynamic and transport properties of isobutane were used in the calculation [31,32]. As the model requires some derivatives of the thermodynamic quantities, our research calculation procedure is presented below in detail.

Mass flux density is given by:

$$G = \frac{\dot{m}_{li}}{A_n} \quad (1)$$

The equilibrium Tangren's adiabatic exponent γ is calculated as:

$$\gamma = \frac{\left[(1 - x_{li}) \frac{c'_p(p_{li})}{c''_p(p_{li})} \right] + 1}{\left[(1 - x_{li}) \frac{c'_p(p_{li})}{c''_p(p_{li})} \right] + \frac{1}{\kappa''_s(p_{li})}} \quad (2)$$

The specific volume of the vapour phase in the nozzle throat is calculated assuming an adiabatic process:

$$v_{nt} = v''(p_{li}) \cdot \left(\frac{p_{nt}}{p_{li}} \right)^{\frac{-1}{\gamma}} \quad (3)$$

The void fraction on the nozzle outlet can be calculated as:

$$\alpha_{li} = \frac{x_{li} v''(p_{li})}{(1 - x_{li}) v'(p_{li}) + x_{li} v''(p_{li})} \quad (4)$$

and the void fraction at the nozzle throat is given by:

$$\alpha_{nt} = \frac{x_{li} v_{nt}}{(1 - x_{li}) v'(p_t) + x_{li} v_{nt}} \quad (5)$$

The equilibrium quality of the two-phase flow in the nozzle throat can be written as:

$$x_{nt} = \frac{s_{li} - s'(p_t)}{s_{fg}(p_t)} \quad (6)$$

In the Henry–Fauske model [30], the empirical parameter E is used. This parameter is dependent on the quality of the fluid x_{nt} at the nozzle throat. For $x_{nt} > 0.14$, parameter $E = 1.0$ is recommended, otherwise the following equation should be used:

$$E = \frac{x_{nt}}{0.14} \quad (7)$$

Additionally, the dimensionless parameter Ω is introduced:

$$\Omega = \frac{1}{\gamma} + \left(1 - \frac{v'(p_{li})}{v_{nt}}\right) \cdot \left[\frac{(1 - x_{li}) E p_t \partial s'(p_t)}{x_{li} s_{fg}(p_t) \partial p_t} \right] - \frac{c''_p(p_{li}) \cdot \left(\frac{1}{\gamma} - \frac{1}{\kappa''_s(p_{li})}\right)}{s_{fg}(p_{li})} \quad (8)$$

The derivative of the specific entropy of the liquid phase $\partial s'(p_t)/\partial p_t$ in Equation (8) is numerically found in the vicinity of the critical pressure. In this paper, it is assumed:

$$\frac{\partial s'(p_t)}{\partial p_t} = \frac{s'(p_t + \Delta p_t) - s'(p_t - \Delta p_t)}{2\Delta p_t} \quad (9)$$

and: $\Delta p_t = 0.01 p_t$. The critical flux density has the following form:

$$G^2 = \left[(1 - x_{li}) v'(p_{li}) \cdot (p_{li} - p_t) + \frac{x_{li} \kappa''_s(p_{li})}{\kappa''_s(p_{li}) - 1} \cdot [p_{li} v''(p_{li}) - p_t v_{nt}] \right] \frac{2}{[(1 - x_{li}) \cdot v'(p_{li}) + x_{li} v_{nt}]^2} \quad (10)$$

As can be seen, for the estimation of the critical mass flux, the value of the critical pressure is required. In the Henry–Fauske model [30], the critical pressure ratio is calculated from the following relationship:

$$\beta = \frac{p_t}{p_{li}} = \left[\frac{\frac{1 - \alpha_{li}}{\alpha_{li}} \left(1 - \frac{p_t}{p_{li}}\right) + \frac{\kappa''_s(p_{li})}{\kappa''_s(p_{li}) - 1}}{\frac{1}{2\Omega \alpha_t^2} + \frac{\kappa''_s(p_{li})}{\kappa''_s(p_{li}) - 1}} \right]^{\frac{\kappa''_s(p_{li})}{\kappa''_s(p_{li}) - 1}} \quad (11)$$

It is the required numerical solution of the above critical pressure p_t implicit equation.

3.2. Analytical Model of the Two-Phase Ejector

The numerical model presented here deals with the mathematical description of the processes occurring in the two-phase ejector. The schematic diagram of the two-phase ejector with its description of the essential cross-sections used in the model is shown in Figure 2. The following assumptions were made:

- Equilibrium phase change;
- The mixing process occurs in the mixing chamber;
- A shock wave occurs after the mixing of both streams, i.e., the motive wet vapour and the entrained superheated vapour;

- Ejector walls are adiabatic;
- The mass, momentum, and energy transfer between the vapour and liquid in the suction chamber are neglected.

In the model presented below, the mass entrainment ratio is assumed, and the unknown parameter is the compression ratio. The geometry of the ejector covers the following main parameters: the nozzle throat diameter D_{nt} ; the nozzle outlet diameter D_{no} ; the mixing chamber diameter D_m ; the mixing chamber length L_m ; the diffuser outlet diameter D_d ; the diffuser length L_d ; and the dimensionless area ratio $\Psi = (D_{nt}/D_m)^2$.

Suction chamber

The pressure in the suction chamber is assumed to be equal to the pressure of the entrained vapour at the inlet to the ejector. As the parameters at the suction chamber inlet are known, the enthalpy h_{vi} and entropy s_{vi} of vapour can be found from the equation of state. The vapour in the suction chamber can be superheated or wet.

In the case of wet vapour, the isentropic quality of the vapour can be found:

$$x_{vs} = \frac{s_{vi} - s'(p_i)}{s_{fg}(p_i)} \quad (12)$$

where p_i is the static pressure at the mixing chamber inlet, and the isentropic enthalpy of the vapour is given by:

$$h_{vs} = h'(p_i) + x_{vs}h_{fg}(p_i) \quad (13)$$

The specific enthalpy in a real process is given by:

$$h_v = h_{vi} - \varphi_s^2(h_{vi} - h_{vs}) \quad (14)$$

where the velocity coefficient of the suction chamber φ_s is assumed as a known quantity. The experimental values of the velocity coefficient φ_s will be found on the basis of our own experimental data.

In the case of wet vapour at the inlet to the ejector, the quality of the vapour is defined as:

$$x_v = \frac{h_v - h'(p_i)}{h_{fg}(p_i)} \quad (15)$$

The density of the entrained wet vapour is given by:

$$\rho_v = [v'(p_i) + x_v v_{fg}(p_i)]^{-1} \quad (16)$$

If the vapour is superheated, the temperature and enthalpy of vapour under isentropic conditions can be found from the equation of state:

$$t_{vs} = t(p_i, s_{vi}) \quad (17)$$

$$h_{vs} = h(p_i, s_{vi}) \quad (18)$$

Equation (14) for specific enthalpy is also valid for superheated vapour; therefore, the density of superheated vapour is:

$$\rho_v = \rho(p_i, h_v) \quad (19)$$

Further calculations are independent of the state of vapour (wet or superheated). The velocity of the vapour at the mixing chamber inlet is equal to:

$$w_v = \varphi_s \sqrt{2(h_{vi} - h_{vs})} \quad (20)$$

from a continuity equation:

$$w_v = \frac{\dot{m}_{vi}}{A_{vi}\rho_v} \quad (21)$$

where A_{vi} is a cross-section area available for the secondary stream, given by:

$$A_{vi} = \frac{\pi}{4} (D_k^2 - D_{no}^2) \quad (22)$$

where D_k is the diameter of the suction chamber in the plane corresponding to the nozzle outlet (see Figure 2). The systems of Equations (20) and (21) can be numerically solved in consideration of the pressure at the mixing chamber inlet p_i .

Motive nozzle

In this model, it is assumed that the pressure p_i is equal to the pressure at the motive nozzle outlet. Depending on the thermodynamic conditions, liquid or wet vapour may emanate from the motive nozzle. As the motive parameters at the nozzle inlet are known, the enthalpy h_{li} and entropy s_{li} of liquid can be found from the equation of state. Thermodynamically, the motive fluid can be delivered as subcooled liquid or wet vapour. It is assumed that two-phase liquid is present at the nozzle outlet. Such conditions occur in every application of the two-phase ejector in refrigeration technology. Therefore, the isentropic quality of wet vapour can be found as follows:

$$x_{ns} = \frac{s_{li} - s'(p_i)}{s_{fg}(p_i)} \quad (23)$$

The specific enthalpy of the motive wet vapour after isentropic expansion is:

$$h_{ns} = h'(p_i) + x_{ns}h_{fg}(p_i) \quad (24)$$

Similarly, it is assumed that the velocity coefficient of the motive nozzle φ_n is known. The experimental values of the velocity coefficient φ_n will be shown in next section. The specific enthalpy of the motive fluid after irreversible expansion is:

$$h_n = h_{li} - \varphi_n^2(h_{li} - h_{ns}) \quad (25)$$

and wet vapour quality is:

$$x_n = \frac{h_n - h'(p_i)}{h_{fg}(p_i)} \quad (26)$$

Neglecting the kinetic energy of the motive fluid at the nozzle inlet, the velocity at the nozzle outlet is given by the following formula:

$$w_n = \sqrt{2(h_{li} - h_n)} \quad (27)$$

and the density is given by the following formula:

$$\rho_n = \left[v'(p_i) + x_n v_{gf} v'(p_i) \right]^{-1} \quad (28)$$

Mixing chamber

In the mixing chamber, the momentum transfer between both streams occurs. After the mixing process, it can be assumed that the flow is homogeneous. The mass velocity in the mixing chamber is:

$$G = \frac{\dot{m}_{li}(1 + U)}{A_m} \quad (29)$$

where: $U = \dot{m}_{vi}/\dot{m}_{li}$. The specific enthalpy under stagnation conditions at the mixing chamber inlet is given by:

$$h_{iz} = \frac{h_{li} + U h_{vi}}{1 + U} \quad (30)$$

and due to the adiabatic-operating conditions of the ejector, this enthalpy h_{iz} is constant. Once again, it is assumed that the velocity coefficient of the mixing chamber φ_m is known. In the presented model, friction between the mixed fluids and the ejector wall is treated separately. Therefore, the calculation of the average parameters of the two-phase flow at the inlet to the mixing chamber is required. The average static enthalpy at the mixing chamber inlet is:

$$h_{mi} = \frac{h_n + U h_v}{1 + U} \quad (31)$$

The average quality in the mixing chamber is given by:

$$x_m = \frac{h_{mi} - h'(p_i)}{h_{fg}(p_i)} \quad (32)$$

and an average density at the mixing chamber inlet is:

$$\rho_i = \left[v'(p_i) + x_m v_{fg}(p_i) \right]^{-1} \quad (33)$$

The dynamic viscosity of the two-phase flow is calculated as:

$$\mu_{tp} = \left(\frac{x_m}{\mu''(p_i)} + \frac{1 - x_m}{\mu'(p_i)} \right)^{-1} \quad (34)$$

and the Reynolds number as:

$$\text{Re}_{tp} = \frac{GD_m}{\mu_{tp}} \quad (35)$$

The flow resistance coefficient is taken from the Blasius equation:

$$f_{tp} = 0.3164 \text{Re}_{tp}^{-0.25} \quad (36)$$

Pressure loss in the mixing chamber can therefore be calculated on the basis of the Darcy–Weisbach formula:

$$\Delta p_f = \frac{1}{2} f_{tp} \frac{L_m}{D_m} \frac{G^2}{\rho_i} \quad (37)$$

The pressure p_m and velocity w_m after mixing should then be calculated. The density of the two-phase system is given by following formula:

$$\rho_m = \left[v'(p_m) + x_m v_{fg}(p_m) \right]^{-1} \quad (38)$$

Therefore, the quality of wet vapour can be found as:

$$x_m(p_m, \rho_m) = \frac{\frac{1}{\rho_m} - v'(p_m)}{v_{fg}(p_m)} \quad (39)$$

and the specific enthalpy after mixing is:

$$h_m(p_m, \rho_m) = h'(p_m) + x_m(p_m, \rho_m) \cdot h_{fg}(p_m) \quad (40)$$

The momentum conservation equation for the mixing process in the cylindrical mixing chamber can be formulated as follows:

$$A_m(p_i - p_m - \Delta p_f) = \dot{m}_{li}(1 + U)w_m - \dot{m}_{li}w_n - \dot{m}_{li}Uw_v \quad (41)$$

The velocity of the two-phase system can be found from the following equation:

$$w_m(p_m) = \frac{1}{\varphi_m} \left(\frac{w_n + Uw_i}{1 + U} - \frac{p_m + \Delta p_f - p_i}{G} \right) \quad (42)$$

Taking into consideration the above, the density is:

$$\rho_m(p_m) = \frac{G}{w_m(p_m)} \quad (43)$$

Using an energy balance equation, the relationship for velocity can be written as:

$$w_m(p_m) = \sqrt{2[h_{iz} - h_m(p_m, \rho_m)]} \quad (44)$$

Combining Equations (42)–(44), the numerical solution of the pressure p_m , velocity w_m , and density ρ_m of wet vapour can be found.

Then, the calculated velocity w_m can be compared with the sonic velocity of the two-phase flow, which we assumed as the following equation:

$$w_s = \sqrt{\frac{1}{[v' + xv_{fg}]^2 \left[\frac{1-x}{[\rho'w'_s]^2} + \frac{x}{[\rho''w''_s]^2} \right]}} \quad (45)$$

Then, the Mach number can be found:

$$Ma_m = \frac{w_m}{w_s} \quad (46)$$

Two-phase mixing shock wave

If the flow in the mixing chamber exceeds sonic velocity, i.e., $Ma_m > 1.0$, then a two-phase mixing shock wave occurs, and the flow will be transformed from supersonic to subsonic. The physical aspects of the forming of a two-phase shock wave may be still thought of as an open research problem. Therefore, it is assumed that similar to the case of a gas shock wave, the thermodynamic properties discretely change across the shock wave. Therefore, it is assumed that the two-phase shock wave shows a discontinuity. Considering the above, the thermodynamic properties of fluid upstream and downstream of the shock wave can be calculated using the systems of the Fanno equation:

$$h_m + \frac{1}{2}v_m^2G^2 = h_t + \frac{1}{2}v_t^2G^2 \quad (47)$$

and Rayleigh equation:

$$p_m + v_mG^2 = p_t + v_tG^2 \quad (48)$$

The static enthalpy after the shock wave is:

$$h_t = h'(p_t) + x_t h_{fg}(p_t) \quad (49)$$

and the specific volume is:

$$v_t = v'(p_t) + x_t v_{fg}(p_t) \quad (50)$$

From the Rayleigh Equation (48), the specific volume of wet vapour can be calculated as:

$$v_t = v_m - \frac{p_t - p_m}{G^2} \quad (51)$$

Combining Equations (50) and (51), it can be written as:

$$x_t(p_t) = \frac{\frac{1}{\rho_m} - v'(p_t) - \frac{p_t - p_m}{G^2}}{v_{fg}(p_t)} \quad (52)$$

Finally, the combination of Equations (47), (50) and (52) gives the following relationship:

$$h_m + \frac{1}{2}v_m^2 G^2 = h_t(p_t) + \frac{1}{2} \left[v_m - \frac{p_t - p_m}{G^2} \right]^2 G^2 \quad (53)$$

The pressure of the mixture after the shock wave p_t can be numerically found from Equation (53). The velocity of the fluid after the shock wave is given by the following formula:

$$w_t = Gv_t \quad (54)$$

Compression in the diffuser

It is assumed in this model that in the diffuser, the velocity of the two-phase homogeneous flow decreases to $w_d = 0$. The velocity coefficient of the diffuser φ_d is assumed as the known parameter. The specific enthalpy of the fluid is also known as this is equal to the stagnation enthalpy:

$$h_d = h_{iz} \quad (55)$$

The momentum conservation equation for the diffuser has the following form:

$$\frac{1}{2}(p_d - p_t)(A_d - A_m) = \dot{m}_{li}(1 + U)w_t\varphi_d \quad (56)$$

where the pressure distribution in the diffuser is assumed as linear. Finally, the ejector outlet pressure can be calculated from the equation:

$$p_d = p_t + 2Gw_t\varphi_d \left(\frac{A_d}{A_m} - 1 \right)^{-1} \quad (57)$$

The overall compression ratio is defined by the equation:

$$\Pi = \frac{p_d - p_{vi}}{p_{li} - p_{vi}} \quad (58)$$

The presented model can be applied for the prediction of the performance of the two-phase ejector, i.e., the compression ratio of the given geometry and assumed efficiencies of the ejector components as well as the entrainment ratio.

Velocity coefficient prediction

As mentioned above, in many theoretical models of the two-phase ejector, the efficiencies of the ejector components should be known. In general, the values of the efficiencies are taken from the literature without any justification, and usually, they are treated as constants. Although the dependence of the efficiency of the ejector components on wet vapour quality is undisputed, the efficiency also depends on the two-phase flow pattern, operating conditions, and duct geometry. The efficiency of the specific components of the ejector can be found from the general relationship: $\eta = \varphi^2$. Therefore, in general, the ejector component efficiencies (and their corresponding velocity coefficients) should not be treated as constants. The correlations of the velocity coefficients of the ejector components are proposed in the next section.

4. Results

4.1. Experimental Assessment of the Critical Flow in the Motive Nozzle

In the experimental investigations of the nozzles of the geometries presented in Table 1 and Figure 3, they were carried out with isobutane as the working fluid. The main goal of the presented investigations was the estimation of the critical mass flux density in the Laval nozzle for the two-phase flows. The experimental results were used also for the validation of the Henry–Fauske model [30] which is usually used in numerous wet steam applications, e.g., the nozzles of the safety valves of steam systems. The experiments were conducted with the control valve closed at the suction line of the ejector during these tests. During the experiments, the pressure and temperature at the nozzle inlet were measured. The outlet parameters were measured in the mixing chamber inlet, and the distance between the nozzle outlet and the first measurement gauge location was 8 mm. Therefore, the outlet parameters of the nozzle should be considered as approximated values. The experimental results of the critical pressure ratio for the experimental and theoretic prediction based on Equation (11) are shown in Figure 4.

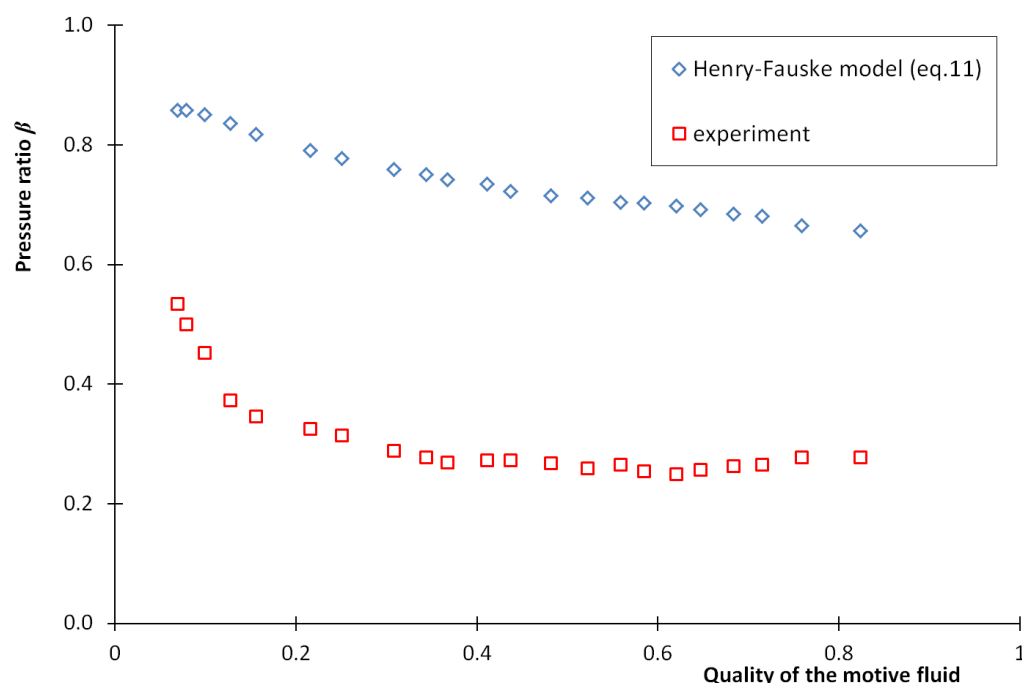


Figure 4. Critical pressure ratio β and experimental pressure ratio vs. quality of wet vapour at the nozzle inlet.

It can be seen that the results of the critical pressure ratio obtained from the Henry–Fauske model indicate that the experimental conditions correspond to the critical flow through the tested motive nozzles as experimental pressure ratio is lower than the critical pressure ratio β . Note that the experimental results correspond to a much lower (by half or more) critical pressure ratio than the numerical prediction according to the model of Henry–Fauske [30]. Therefore, the Henry–Fauske model [30] can be used for the validation of the critical flux density for isobutane as a working fluid under the considered test conditions.

Figure 5 shows the comparison of the relationship between the mass flux density and wet vapour quality obtained experimentally and predicted with the use of the Henry–Fauske model. As it can be seen from Figure 5, the critical mass flux is, in general, underpredicted by the Henry–Fauske model. However, it can be seen that the Henry–Fauske model much more accurately predicts the experimental results of the higher quality of motive fluid. For $x_{ji} > 0.65$, the predicted results can be considered as very accurate in comparison with the experimental results, i.e., the average difference between the theoretical and measured values is less than $\pm 5\%$.

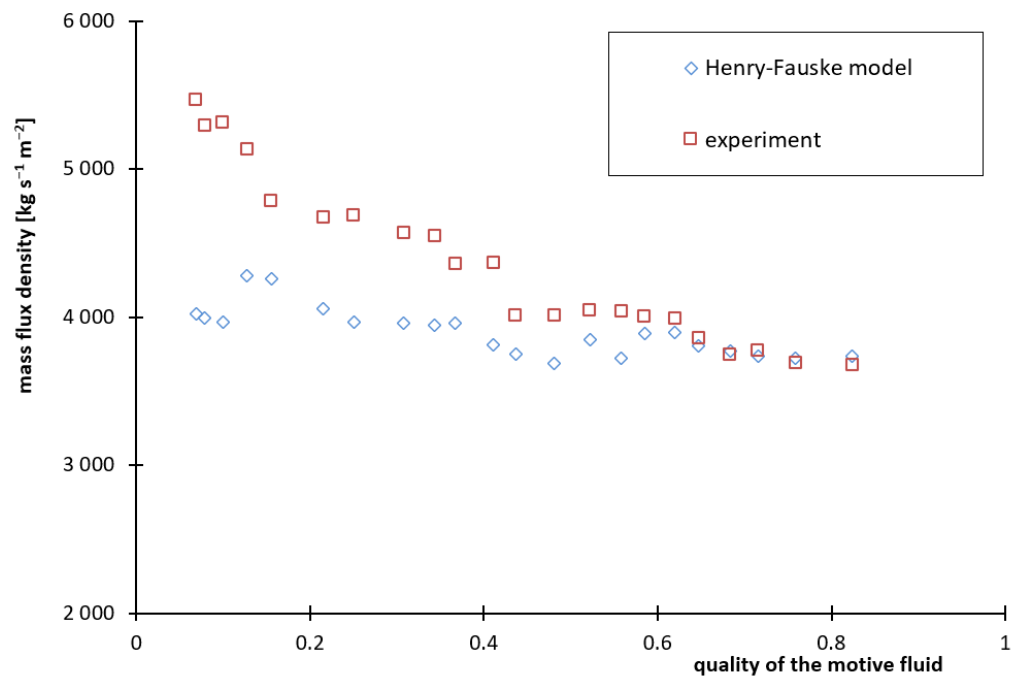


Figure 5. Mass flux density vs. quality of wet vapour at the nozzle inlet.

4.2. Coefficient of the Velocity of the Two-Phase Motive Nozzles

The velocity coefficient is defined as a ratio of the velocity at the nozzle outlet w_n to the velocity at the nozzle outlet under isentropic conditions w_{ns} :

$$\varphi_n = \sqrt{\eta_n} = \frac{w_n}{w_{ns}} \quad (59)$$

The estimation of the velocity coefficient of the nozzles operating with wet vapour may not be thought of as a standard issue as the outlet fluid parameters are unknown, and especially the quality of the wet vapour at the nozzle outlet x may not be directly measured. Our own approach in terms of the assessment of the velocity coefficient of the two-phase nozzle is presented below.

For the given inlet parameters and outlet pressure, the isentropic velocity is given by following formula:

$$w_{ns} = \sqrt{2(h_{li} - h_{ns})} \quad (60)$$

where h_{ns} is the specific enthalpy of the fluid at the isentropic nozzle outlet. The kinetic energy of the fluid at the nozzle inlet was neglected in Equation (60). The isentropic mass velocity is given by formula:

$$w_{ns}\rho_{ns} = \dot{G}_s \quad (61)$$

The theoretical mass flow rate is compared with the measured mass flow rate given by:

$$\dot{m}_{li} = A_{no}\rho_n w_n \quad (62)$$

where A_{no} is the area of the nozzle outlet. The mass velocity under experimental conditions can be calculated as follows:

$$\dot{G} = \frac{\dot{m}_{li}}{A_{no}} = \rho_n w_n \quad (63)$$

Therefore, the ratio of the mass velocities can be calculated:

$$\psi_n = \frac{\dot{G}}{\dot{G}_s} = \frac{\rho_n w_n}{\rho_{ns} w_{ns}} \quad (64)$$

Equation (64) can be written in another form:

$$\psi_n = \frac{\rho_n}{\rho_{ns}} \varphi_n \quad (65)$$

Therefore, the velocity coefficient can be written as:

$$\varphi_n = \psi_n \frac{\rho_{ns}}{\rho_n} \quad (66)$$

where the density of the wet vapour is given by:

$$\rho_n = \left[v'(p_n) + x_n h_{fg}(p_n) \right]^{-1} \quad (67)$$

In Equation (67), the quality x_n is an unknown parameter. However, using the energy equation for the inlet and outlet cross-sections of the nozzle, the velocity coefficient can be written in the following form:

$$\varphi_{nh} = \sqrt{\frac{h_{li} - h_n}{h_{li} - h_{ns}}} \quad (68)$$

where the specific enthalpy of wet vapour can be found as:

$$h_n = h'(p_n) + x_n h_{fg}(p_n) \quad (69)$$

The quality of the wet vapour at the nozzle exit can be found with the numerical solution of the equation:

$$\varphi_n(x_n) = \varphi_{nh}(x_n) \quad (70)$$

After the calculation of the wet vapour quality x_n , the velocity coefficient of the two-phase nozzle can be found using Equation (68).

On the basis of the experimental results of all of the nozzles presented in Table 1 and Figure 3, the relationship between the velocity coefficient φ_n and the quality of the fluid at the nozzle outlet x_n can be found. This relationship is presented in Figure 6.

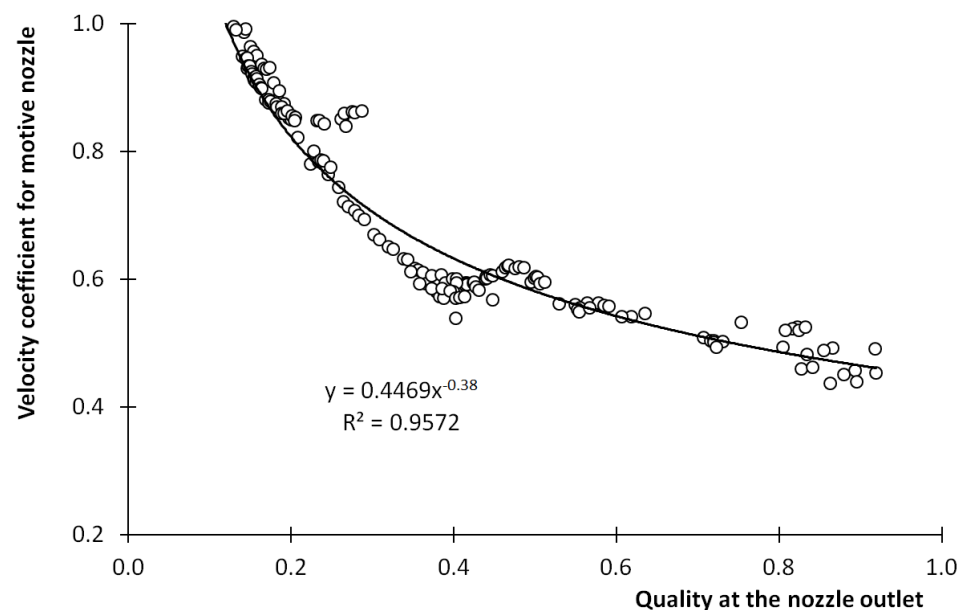


Figure 6. Velocity coefficient of motive nozzle vs. wet vapour quality at the nozzle outlet.

The experiments show that the velocity coefficient of the tested nozzle covers the range $0.3 < \varphi_n < 1.0$ in the full range of wet vapour quality. However, most of the experimental

results show that the quality of the fluid at the nozzle outlet was lower than 0.50. The proposed correlation of the velocity coefficient has the following form:

$$\varphi_n = C_{n0} + C_{n1}x_{ns}^{C_{n2}} \quad (71)$$

The systematic experimental results of the investigation of the nozzles with various geometry (Table 1) were used in the determination of the constants $C_{n0} = 0$, $C_{n1} = 0.4469$, and $C_{n2} = -0.38$.

As it can be seen in Figure 7, the numerical results obtained from the correlation given by Equation (60), in most cases, correspond very well to the experimental data. The discrepancy is $\pm 15\%$, and it results from the different operation of the nozzles.

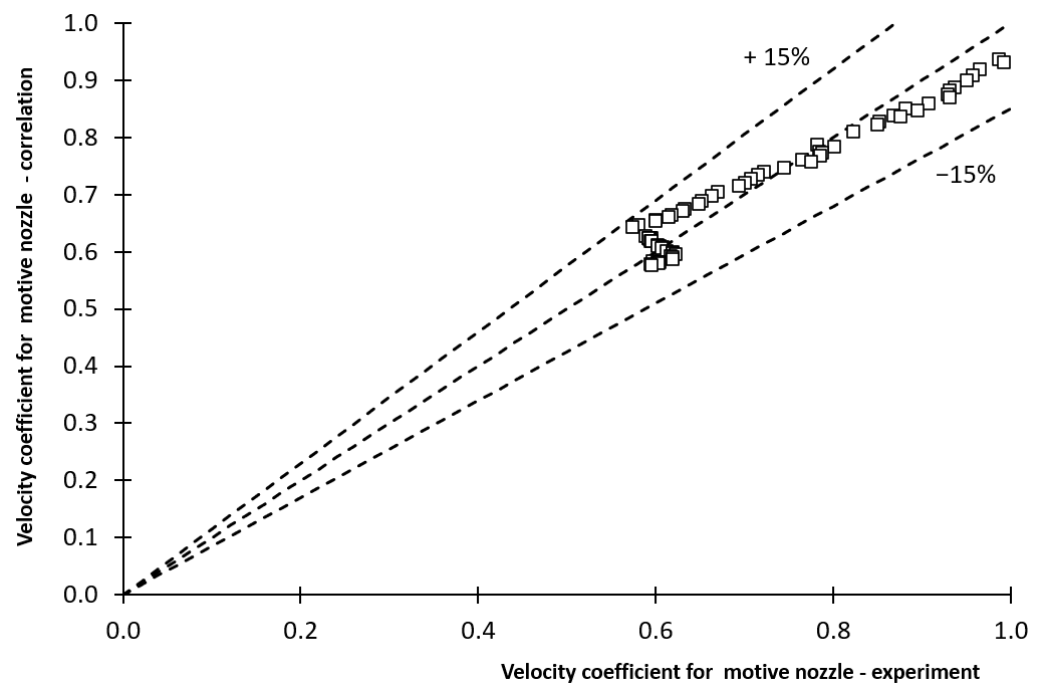


Figure 7. Calculated velocity coefficient vs. experimental velocity coefficient.

4.3. Coefficient of the Velocity of the Suction Chamber

The velocity coefficient of the suction chamber was numerically calculated for experimental data according to Equations (20) and (21). The Experimental data demonstrate that the velocity coefficient is correlated with the volumetric entrainment ratio and the distance between the motive nozzle outlet and the mixing chamber inlet. It is seen that the relationship between the velocity coefficient φ_s of the suction chamber and the volumetric entrainment ratio χ is linear. Therefore, the final form of the correlation of the velocity coefficient was obtained:

$$\varphi_s = (0.06907 - 0.05149 \Lambda)\chi \quad (72)$$

where: $\Lambda = L_{no}/D_m$, and L_{no} is the distance between the nozzle outlet and the mixing chamber inlet.

The results presented in Figure 8 show that the velocity coefficient of the suction chamber is relatively small and does not exceed $\varphi_s = 0.35$, which indicates a low efficiency of the suction chamber. The velocity coefficient increases proportionally to the entrainment ratio. The volumetric entrainment ratio χ varies between 0 and 8.0. The relation of the velocity coefficient of the geometry parameter $\varphi_s = f(\Lambda)$ is inversely proportional, e.g., for the highest geometry parameter $\Lambda = 0.750$, the velocity coefficient varies between 0.10–0.13 for $\chi = 4.0$, and for the lowest geometry parameter $\Lambda = 0.417$, the velocity coefficient exceeds the highest values and varies between 0.17–0.25 for the same volumetric entrainment ratio

$\chi = 4.0$. The comparison of the calculated velocity coefficient (Equation (72)) with the experimental velocity coefficient is shown in Figure 9.

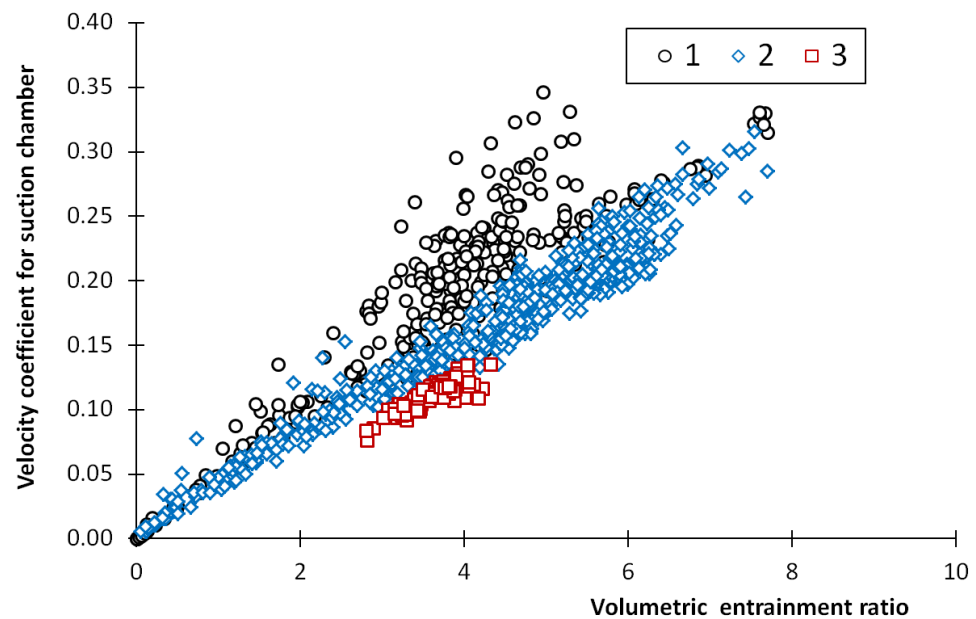


Figure 8. Velocity coefficient of suction chamber vs. volumetric entrainment ratio: (1) $\Lambda = 0.417$; (2) $\Lambda = 0.583$; and (3) $\Lambda = 0.750$.

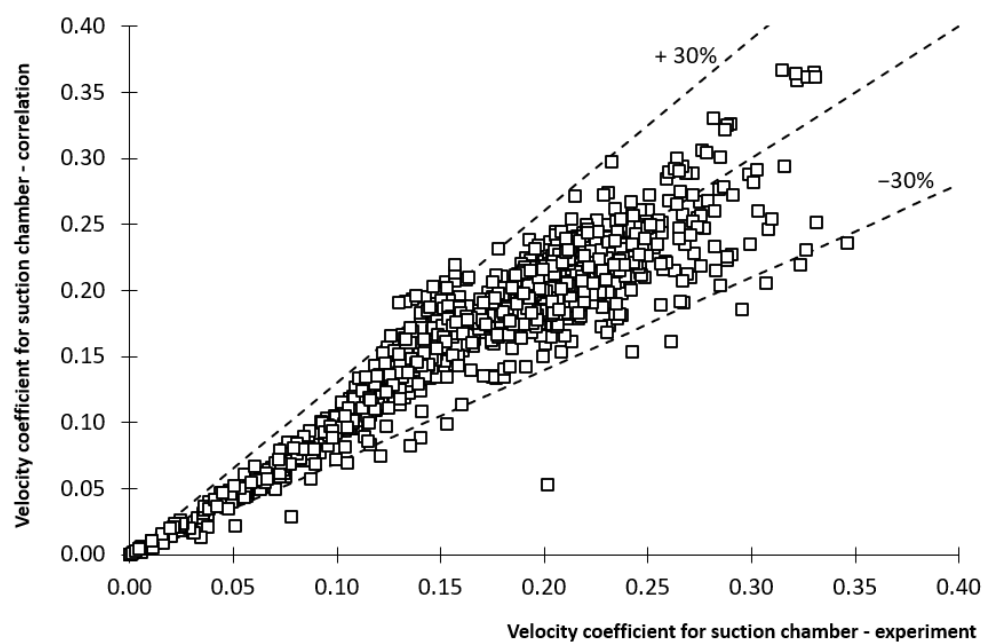


Figure 9. Calculated velocity coefficient vs. experimental velocity coefficient.

It can be seen from Figure 9 that the calculated velocity coefficient of the suction chamber achieves good agreement with the experimental results. Excluding some individual cases, the discrepancy of the results is less than 30% for the proposed correlation. It should be also taken into account that in most cases, a kind of froth two-phase flow occurs in the mixing chamber as a result of the partially reverse flow phenomena at the entrance to the mixing chamber. These phenomena are the reason for the complicated flow pattern which causes some discrepancies of the velocity coefficient. In addition, these phenomena are responsible for the significant losses of momentum in the suction chamber which result in rather a low level of the measured coefficient of velocity.

4.4. Coefficient of the Velocity of the Mixing Chamber

The experimental data demonstrate that the velocity coefficient is correlated with the volumetric entrainment ratio χ and geometry parameter Ψ , which is shown in Figure 10. The correlation of the mixing chamber velocity coefficient was proposed in the following form:

$$\varphi_m = (0.03747 + 0.08462\Psi)\chi \quad (73)$$

The obtained experimental results demonstrate that the relationship between the velocity coefficient φ_m of the mixing chamber and the volumetric entrainment ratio χ is linear and proportionally increases up to $\varphi_m = 0.35$, with the volumetric entrainment ratio increasing up to $\chi = 8.0$; see Figure 10. Based on the results shown in Figure 10, it can be seen that, in general, the ejector of the geometry parameter $\Psi = 0.0278$ exceeds the slightly lower values of the velocity coefficient than the ejector of the geometry parameter $\Psi = 0.0625$ for the same volumetric entrainment ratio. The ejector of the geometry parameter $\Psi = 0.111$, in general, operates with a low entrainment ratio $\chi < 3.0$, and the velocity coefficient exceeds the same values $\varphi_m < 0.13$ as in the case of the other tested geometries.

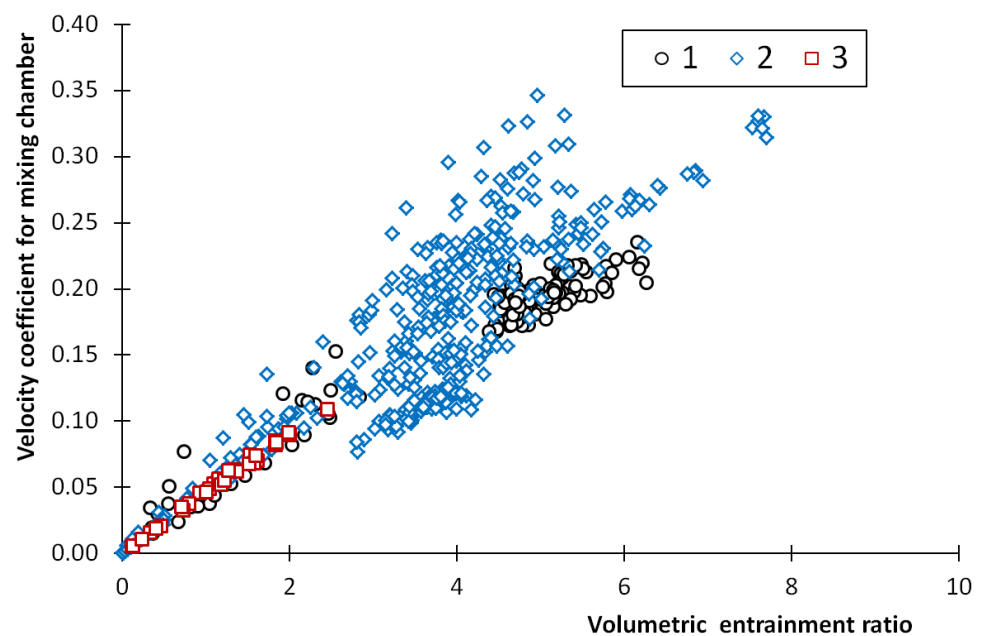


Figure 10. Velocity coefficient of the mixing chamber vs. volumetric entrainment ratio: (1) $\Psi = 0.0278$; (2) $\Psi = 0.0625$; and (3) $\Psi = 0.111$.

The comparison of the calculated velocity coefficient Equation (73) with the experimental velocity coefficient is shown in Figure 11. It can be seen from Figure 11 that the calculated velocity coefficient of the mixing chamber agrees well with experimental results. Once again, excluding some individual cases, the discrepancy of the results is less than 30% for the proposed correlation. It should be noted that as a consequence of the complicated flow pattern inside the mixing chamber, the obtained accuracy may be thought of as reasonably good.

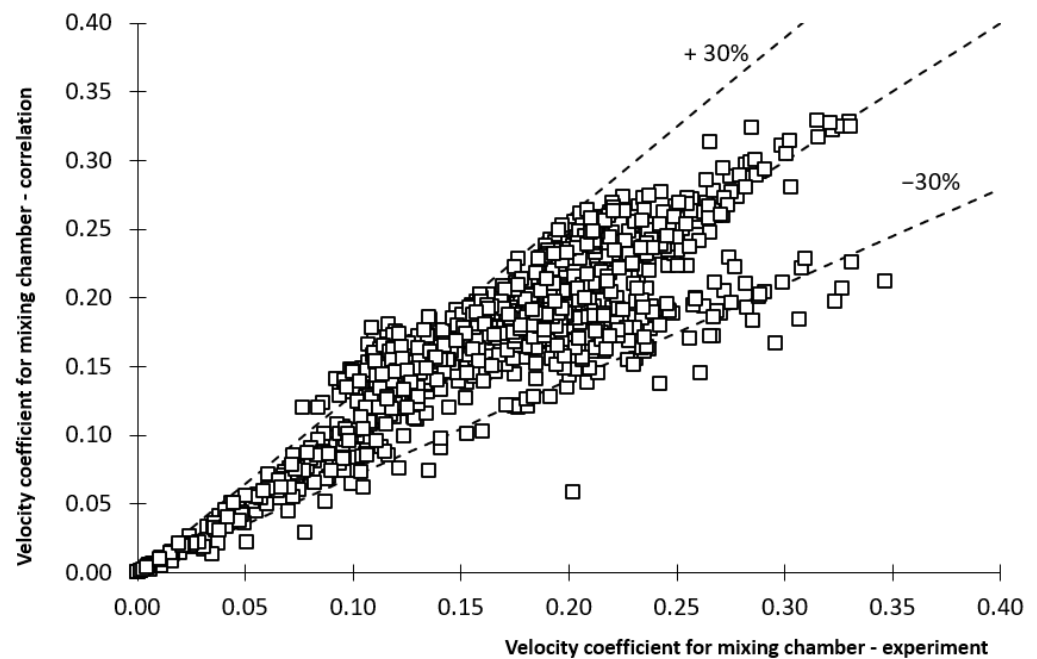


Figure 11. Calculated velocity coefficient of the mixing chamber vs. experimental velocity coefficient.

4.5. Coefficient of the Velocity of the Diffuser

The velocity coefficient of the diffuser can be directly found from Equation (57). It is worth noting that the diffuser in a two-phase ejector does not play a major role as the effect of the compression is obtained due to the shock wave rather than the operation of the diffuser. Therefore, in some cases, if the shock wave produces a high pressure lift, there can be observed an even slight decrease in the static pressure in the diffuser. This phenomenon is caused by friction pressure losses, flow detachment, and vortices that occur in the diffuser. Therefore, the diffuser operation and its efficiency can be considered as a rather random quantity that depends on numerous parameters.

Once again, taking into consideration the geometry parameter Ψ and operation parameters, i.e., the volumetric entrainment ratio χ of the two-phase ejector, the relationship between those parameters and the velocity coefficient of the diffuser φ_{dk} is shown in Figure 12. Therefore, the correlation of the velocity coefficient in a linear form is proposed:

$$\varphi_{dk}(\chi, \Psi) = (0.075 + 0.108\Psi)\chi \quad (74)$$

The experiment shows that for the tested ejector of the geometry parameter Ψ , the velocity coefficients are, in general, lower than $\varphi_{dk} < 0.40$. The proportional relationship between the velocity coefficient and the entrainment ratio can be observed. Despite the large discrepancy of the results, it can be seen that for the ejector of the geometry parameter $\Psi = 0.0625$, the efficiency of the diffuser is slightly better than with the geometry parameter $\Psi = 0.0278$. The lowest efficiency of the diffuser is observed for the ejector with the geometry parameter $\Psi = 0.111$. In this case, the velocity coefficient is lower than 10%, $\varphi_{dk} < 0.10$. The comparison of the calculated velocity coefficients on the basis of Equation (74) with experimentally obtained velocity coefficients is shown in Figure 13.

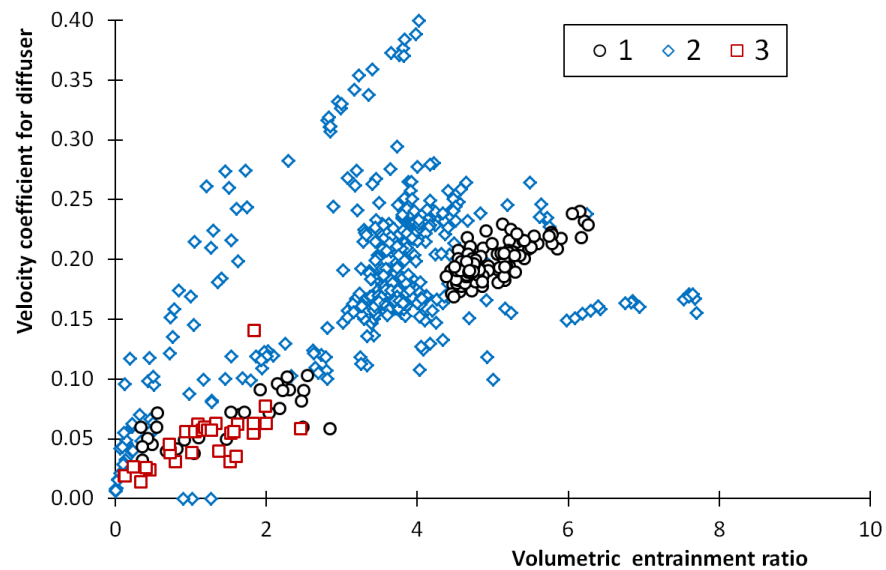


Figure 12. Velocity coefficient of the diffuser vs. volumetric entrainment ratio: (1) $\Psi = 0.0278$; (2) $\Psi = 0.0625$; and (3) $\Psi = 0.111$.

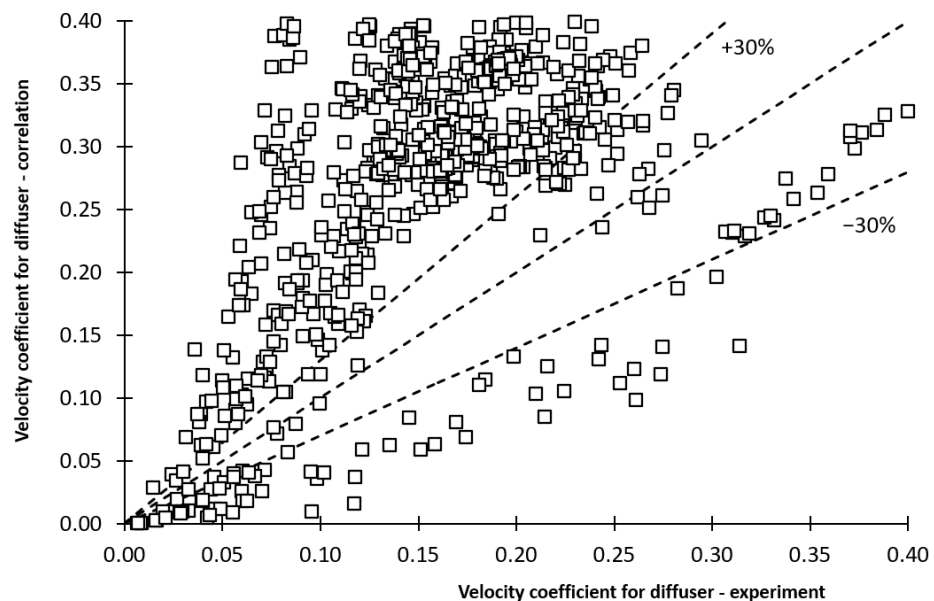


Figure 13. Calculated velocity coefficient of diffuser vs. experimental velocity coefficient.

It is seen in Figure 13 that the adjustment of the calculated velocity coefficients and the experimental values can be considered as relatively good. However, the diffuser is the ejector component of the smallest efficiency; therefore, the pressure lift in the diffuser is, in many cases, rather minor. By the nature of the flow inside the diffuser, the determination of the velocity coefficient of this component of the two-phase injector for the entire range of the operation conditions is thought to be a very complex and problematic task due to the large discrepancy and randomness of the results.

5. Conclusions

Based on the presented results, the following conclusion can be drawn:

1. The mathematical model of the processes occurring in a two-phase ejector based on balance equations is presented. The model assumes the ejector geometry and inlet pressures and temperatures as well as the entrainment ratio to be known. The model

can predict the pressure increase in a two-phase ejector. The coefficients of velocity could be determined on the basis of the experimental data using the formulated model. It was demonstrated that the coefficients of velocities may not be considered as constant quantities for the two-phase ejector.

2. Based on the experimental results of the ejector with various geometry described by the geometrical parameters Λ and Ψ , the correlations of the velocity coefficients of the components of the ejector were proposed. The quality of fluid x in the case of the motive nozzle and the volumetric entrainment ratio χ for other ejector components were selected as the parameters that affect, to the maximum extent, the experimentally obtained velocity coefficients. For the components of the ejector, the velocity of the coefficients lower than 0.4 was obtained for the tested ejector and operation conditions. Except for the motive nozzle, the linear proportional relationship between the velocity coefficient and entrainment ratio was found. The numerical results based on the proposed correlations fit with the experimental data within 30%.
3. The experiments were conducted using a wide range of operating parameters showing the applicability of the Henry–Fauske model [30] to predict the critical mass flow rate in the case of isobutane wet vapour. However, this model can predict the critical mass flow rate very accurately (with discrepancy $\pm 5\%$) in the case of isobutane for a wet vapour quality higher than 0.65 at the inlet to the nozzle, and for a lower quality of wet vapour, this model underpredicts the experimental data by as much as 20%.

Author Contributions: Data curation, K.Ś., J.G. and P.J.; Investigation, A.D.; Methodology, D.B.; Supervision, H.Z.; Writing—original draft, K.Ś.; Writing—review & editing, D.B. All authors have read and agreed to the published version of the manuscript.

Funding: The research results presented in the paper were completed within the statutory activities WZ/WM-IIM/1/2020, financed by the Ministry of Education and Science, and supported by Białystok University of Technology research project no. WI/WM-IIM/8/2020.

Institutional Review Board Statement: Not applicable.

Informed Consent Statement: Not applicable.

Data Availability Statement: Not applicable.

Conflicts of Interest: The authors declare no conflict of interest.

Nomenclature

A	surface area, m^2
C	constant
c	specific heat capacity, $J/(kg \cdot K)$
D	diameter, m
f	flow resistance coefficient
G	mass flux density, $kg/(m^2 \cdot s)$
h	specific enthalpy, J/kg
L	length, m
\dot{m}	mass flow rate, kg/s
Ma	Mach number
p	pressure, Pa
Re	Reynolds number
s	specific entropy, $J/(kg \cdot K)$
t	temperature, $^{\circ}C$
U	mass entrainment ratio
w	velocity, m/s
v	specific volume, m^3/kg
x	wet vapour quality

Greek symbols

γ	adiabatic exponent
ρ	density, kg/m ³
η	efficiency
κ	isentropic exponent
Λ	geometrical parameter, $\Lambda = L/D$
μ	dynamic viscosity, Pa·s
Π	compression ratio
φ	velocity coefficient
χ	volumetric entrainment ratio
Ψ	surface area ratio
Ω	model parameter in Equation (8)

Subscripts and superscripts

<i>d</i>	diffuser
<i>e</i>	equilibrium
<i>fg</i>	vaporisation
<i>i</i>	inlet
<i>iz</i>	stagnation condition
<i>l</i>	liquid
<i>li</i>	inlet of the liquid phase
<i>m</i>	mixing chamber
<i>nt</i>	nozzle throat
<i>no</i>	nozzle outlet
<i>o</i>	outlet
<i>s</i>	isentropic process; suction chamber
<i>t</i>	throat; after shock wave
<i>tp</i>	two-phase
<i>v</i>	vapour
<i>vi</i>	inlet of entrained vapour
'	saturated liquid
''	saturated vapour

References

1. Yadav, V.K.; Sarkar, J.; Ghosh, P. Thermodynamic, economic and environmental analyses of novel solar-powered ejector refrigeration systems. *Energy Convers. Manag.* **2022**, *264*, 115730. [[CrossRef](#)]
2. Sutthivirode, K.; Thongtip, T. Experimental investigation of a two-phase ejector installed into the refrigeration system for performance enhancement. *Energy Rep.* **2022**, *8*, 7263–7273. [[CrossRef](#)]
3. Besagni, G.; Mereu, R.; Inzoli, F. Ejector refrigeration: A comprehensive review. *Renew. Sustain. Energy Rev.* **2016**, *53*, 373–407. [[CrossRef](#)]
4. Haider, M.; Elbel, S. Development of ejector performance map for predicting fixed-geometry two-phase ejector performance for wide range of operating conditions. *Int. J. Refrig.* **2021**, *128*, 231–241. [[CrossRef](#)]
5. Bauzvand, A.; Tavousi, E.; Noghrehabadi, A.; Behbahani-Nejad, M. Study of a novel inlet geometry for ejectors. *Int. J. Refrig.* **2022**, *139*, 113–127. [[CrossRef](#)]
6. Li, Y.; Yu, J. The effects of ejector geometry parameter and refrigerant charge amount on an ejector-expansion refrigeration system. *Appl. Therm. Eng.* **2019**, *125*, 402–408. [[CrossRef](#)]
7. Ameer, K.; Aidoun, Z. Two-phase ejector enhanced carbon dioxide transcritical heat pump for cold climate. *Energy Convers. Manag.* **2021**, *243*, 114421. [[CrossRef](#)]
8. Zhu, Y.; Li, C.; Zhang, F.; Jiang, P. Comprehensive experimental study on a transcritical CO₂ ejector-expansion refrigeration system. *Energy Convers. Manag.* **2017**, *151*, 98–106. [[CrossRef](#)]
9. Zheng, L.; Deng, J. Experimental investigation on a transcritical CO₂ ejector expansion refrigeration system with two-stage evaporation. *Appl. Therm. Eng.* **2017**, *125*, 919–927. [[CrossRef](#)]
10. He, Y.; Deng, J.; Li, Y.; Zhang, X. Synergistic effect of geometric parameters on CO₂ ejector based on local exergy destruction analysis. *Appl. Therm. Eng.* **2021**, *184*, 116256. [[CrossRef](#)]
11. Haida, M.; Palacz, M.; Bodys, J.; Smolka, J.; Gullo, P.; Nowak, A.J. An experimental investigation of performance and instabilities of the R744 vapour compression rack equipped with a two-phase ejector based on short-term, long-term and unsteady operations. *Appl. Therm. Eng.* **2021**, *85*, 116353. [[CrossRef](#)]

12. Palacz, M.; Haida, M.; Smolka, J.; Nowak, A.J.; Banasiak, K.; Hafner, A. HEM and HRM accuracy comparison for the simulation of CO₂ expansion in two-phase ejectors for supermarket refrigeration systems. *Appl. Therm. Eng.* **2017**, *115*, 160–169. [[CrossRef](#)]
13. Zhang, Z.; Feng, X.; Tian, D.; Yang, J.; Chang, L. Progress in ejector-expansion vapor compression refrigeration and heat pump systems. *Energy Convers. Manag.* **2020**, *207*, 112529. [[CrossRef](#)]
14. İşkan, U.; Direk, M. Experimental performance evaluation of the dual-evaporator ejector refrigeration system using environmentally friendly refrigerants of R1234ze(E), ND, R515a, R456a, and R516a as a replacement for R134a. *J. Clean. Prod.* **2022**, *352*, 131612. [[CrossRef](#)]
15. Li, H.; Cao, F.; Bu, X.; Wang, L.; Wang, X. Performance characteristics of R1234yf ejector-expansion refrigeration cycle. *Appl. Energy* **2014**, *121*, 96–103. [[CrossRef](#)]
16. Sag, N.B.; Ersoy, H.K.; Hepbasli, A.; Halkaci, H.S. Energetic and exergetic comparison of basic and ejector expander refrigeration systems operating under the same external conditions and cooling capacities. *Energy Convers. Manag.* **2015**, *90*, 184–194. [[CrossRef](#)]
17. Taleghani, S.T.; Sorin, M.; Poncet, S. Modeling of two-phase transcritical CO₂ ejectors for on-design and off-design conditions. *Int. J. Refrig.* **2018**, *87*, 91–105. [[CrossRef](#)]
18. Jeon, Y.; Jung, J.; Kim, D.; Kim, S.; Kim, Y. Effects of ejector geometries on performance of ejector-expansion R410A air conditioner considering cooling seasonal performance factor. *Appl. Energy* **2017**, *205*, 761–768. [[CrossRef](#)]
19. Butrymowicz, D.; Smierciew, K.; Regulska, D.; Karwacki, J.; Trela, M. Experimental investigation of effect of motive nozzle diameter on performance of liquid-vapour ejector. In Proceedings of the International Seminar on Ejector/ Jet-Pump Technology and Application, Louvain-La-Neuve, Belgium, 7–9 September 2009. Paper No. 24.
20. Ringstad, K.E.; Banasiak, K.; Ervik, A.; Hafner, A. Machine learning and CFD for mapping and optimization of CO₂ ejectors. *Appl. Therm. Eng.* **2021**, *199*, 117604. [[CrossRef](#)]
21. Wilhelmsen, Ø.; Aasen, A.; Banasiak, K.; Herlyng, H.; Hafner, A. One-dimensional mathematical modeling of two-phase ejectors: Extension to mixtures and mapping of the local exergy destruction. *Appl. Therm. Eng.* **2022**, *217*, 119228. [[CrossRef](#)]
22. Ameer, K.; Aidoun, Z.; Ouzzane, M. Modeling and numerical approach for the design and operation of two-phase ejectors. *Appl. Therm. Eng.* **2016**, *109*, 809–818. [[CrossRef](#)]
23. Banasiak, K.; Palacz, M.; Hafner, A.; Bulinski, Z.; Smolka, J.; Nowak, A.; Fic, A. A CFD-based investigation of the energy performance of two-phase R744 ejectors to recover the expansion work in refrigeration systems: An irreversibility analysis. *Int. J. Refrig.* **2014**, *40*, 328–337. [[CrossRef](#)]
24. Yazdani, M.; Alahyari, A.A.; Radcliff, T.D. Numerical modeling of two-phase supersonic ejectors for work-recovery applications. *Int. J. Heat Mass Transf.* **2012**, *55*, 5744–5753. [[CrossRef](#)]
25. Zhu, Y.; Huang, Y.; Li, C.; Zhang, F.; Jiang, P. Experimental investigation on the performance of transcritical CO₂ ejector–expansion heat pump water heater system. *Energy Convers. Manag.* **2018**, *167*, 147–155. [[CrossRef](#)]
26. Lu, Y.; Bai, T.; Yu, J. Experimental investigation on a –40 °C low-temperature freezer using ejector-expansion refrigeration system. *Int. J. Refrig.* **2020**, *118*, 230–237. [[CrossRef](#)]
27. Chaiwongsa, P.; Wongwises, S. Experimental study on R-134a refrigeration system using a two-phase ejector as an expansion device. *Appl. Therm. Eng.* **2008**, *28*, 467–477. [[CrossRef](#)]
28. Lawrence, N.; Elbel, S. Experimental investigation of a two-phase ejector cycle suitable for use with low-pressure refrigerants R134a and R1234yf. *Int. J. Refrig.* **2014**, *38*, 310–322. [[CrossRef](#)]
29. Sumeru, K.; Sulaimon, S.; Nasution, H.; Ani, F.N. Numerical and experimental study of an ejector as an expansion device in split-type air conditioner for energy savings. *Energy Build.* **2014**, *79*, 98–105. [[CrossRef](#)]
30. Henry, R.E.; Fauske, H.K. The two-phase critical flow of one-component mixtures in nozzles, orifices, and short tubes. *ASME J. Heat Transfer* **1971**, *93*, 179–187. [[CrossRef](#)]
31. Lemmon, E.W.; Huber, M.L.; McLinden, M.O. *NIST Standard Reference Database 23: Reference Fluid Thermodynamic and Transport Properties-REFPROP*, version 9.1; National Institute of Standards and Technology: Gaithersburg, MD, USA, 2013; Standard Reference Data Program.
32. Bücker, D.; Wagner, W. Reference equations of state for the thermodynamic properties of fluid phase n-butane and isobutane. *J. Phys. Chem. Ref. Data* **2006**, *35*, 929–1019. [[CrossRef](#)]